

USE AND ABUSE OF EIS IN STUDYING THE MECHANISMS OF CO₂/H₂S CORROSION OF MILD STEEL

Kun-Lin John Lee and Srdjan Nešić
Ohio University
Institute for Corrosion and Multiphase Flow Technology
342 West State Street
Athens, OH 45701
USA

ABSTRACT

Electrochemical Impedance Spectroscopy (EIS) is a powerful transient technique which enables an insight into the corrosion process not easily obtained by other predominantly DC techniques. However the EIS technique presents a large challenge both from a theoretical as well as an experimental point of view. Collecting accurate EIS raw data is not easy as EIS is plagued with errors not seen by the DC techniques. Building mechanistic models to capture the EIS data is a very complex task which enables extraction of valuable information about the corrosion process, however the time and effort investment required is very large.

In this study of CO₂/H₂S corrosion of mild steel it was found that a “minor” detail in the experimental set-up caused erroneous acquisition of EIS raw data. These data were “successfully” modeled by using a complex electrochemical theory, which appeared plausible. When the experimental mistake was discovered the EIS data were retaken, the analysis was redone and the conclusions about the corrosion process were completely revised.

Keywords: EIS, mechanism, CO₂/H₂S corrosion, mild steel

INTRODUCTION

For many years, the vast majority of electrochemical studies of mild steel in CO₂ solutions (with and without H₂S) have been confined to traditional steady state techniques such as linear polarization resistance (LPR) and potentiodynamic sweep (PS) measurements. However, steady-state techniques are limited when they are used for

analyzing corrosion processes because they only give information on the rate-determining step. When corrosion involves multiple steps, steady-state techniques are not adequate to elucidate the reaction mechanism. Moreover, during the measurement process, techniques such as potentiodynamic sweep polarize the electrode surface to such an extent that it is debatable if the measurement results are valid since the surface conditions change significantly during the measurement. In $\text{CO}_2/\text{H}_2\text{S}$ corrosion of steel it was found that large degree of polarization disturbed the corroding system irreversibly during the measuring process.

On the other hand, a transient electrochemical technique such as Electrochemical Impedance Spectroscopy (EIS), is less intrusive than potentiodynamic sweep technique, because its underlying principle is to disturb the reaction from the steady state by applying small amplitude sinusoidal perturbation to the electrochemical system. As the various elementary processes change at different rates, their responses to the perturbation can be obtained at different frequencies in a single experiment. Therefore EIS is a powerful diagnostic method for analyzing $\text{CO}_2/\text{H}_2\text{S}$ corrosion mechanisms involving multiple charge transfer steps with adsorbed intermediates at the metal surface. No systematic studies on $\text{CO}_2/\text{H}_2\text{S}$ corrosion have been made using the EIS technique. In this study the mechanism and kinetics of corrosion process in saturated CO_2 solution with and without H_2S was investigated using the EIS technique.

Due to the difficulty in extracting meaningful physical information from the Nyquist plot produced by using EIS technique, an analytical tool is required in order to interpret the mechanisms. Traditionally, equivalent circuit analysis was commonly used to interpret the information from the Nyquist plot by fitting the data with a combination of capacitors, resistors and inductors. However, this approach is not conclusive in determining the mechanism because various combinations of equivalent circuit can all lead to a similar results. Furthermore, equivalent circuit analysis provides very limited information on the underlying physico-chemical process. Therefore, a more mechanistic approach was pursued here and a model built to interpret EIS data that gives an electrochemical impedance response based on fundamental equation of electrochemistry. This mechanistic model was able to fit complicated EIS curves and provide qualitative and quantitative information of the underlying $\text{CO}_2/\text{H}_2\text{S}$ corrosion process.

EXPERIMENT

In order to determine the mechanism and the missing physical constants for $\text{H}_2\text{S}/\text{CO}_2$ corrosion, experiments were conducted in a glass cell on API 5L X65 carbon steel at these conditions: $T=20^\circ\text{C}$, $\text{pH}5$, $P=1$ bar, gaseous H_2S concentration in $\text{CO}_2 = 0, 3, 15, 100$ and 250 ppm, $\omega = 1000$ rpm. In these experiments the corrosion process was monitored with different electrochemical measuring techniques: Electrochemical Impedance Spectroscopy (EIS) and Linear Polarization Resistance (LPR). Experiment for each H_2S concentration was conducted at least twice to make sure the result was reproducible and reliable.

Equipment

Experiments were conducted at atmospheric pressure in a glass cell at room temperature. Gas (different concentration of H₂S in CO₂) was continuously bubbled through the cell. A three-electrode set-up (Figure 1) was used in all electrochemical experiments. A rotating cylinder electrode with a speed control unit was used as the working electrode. A concentric platinum ring was used as a counter electrode. A saturated Ag/AgCl reference electrode was used externally connected to the cell via a Luggin capillary and a porous wooden plug. The pH was followed with an electrode directly immersed into the electrolyte. H₂S and CO₂ gas was scrubbed by NaOH absorbent. Electrochemical measurements were made with a potentiostat connected with a computer.

Material

A typical construction API 5L X65 carbon steel was tested. Chemical composition of the steel is given in Table 1. The working electrode was machined from the parent material into a cylinder 12 mm in diameter and 14.3 mm long. The exposed area of the specimen was 5.4 cm².

Experimental Procedure

The glass cell was filled with 2 liters of electrolyte: de-ionized distilled water + 3 mass% NaCl. Initially CO₂ gas was bubbled through the electrolyte (at least one hour prior to experiments) in order to saturate and deaerate the solution. Monitoring of pH was used to determine whether the solution is in equilibrium. In different experiments various concentration of H₂S in CO₂ gas were then bubbled through the electrolyte (at least 1 hour) in order to saturate the solution. The gaseous concentration of H₂S was verified by color metric tube. A strong solution of NaHCO₃ was deaerated with CO₂ before some was added to the cell to adjust the solution to pH5. The steel working electrode surface was then polished with 220 and 600 grit silicon carbide paper, washed with alcohol, mounted on the specimen holders and immersed into the electrolyte. The free corrosion potential was followed immediately after immersion. Linear Polarization Resistance (LPR) technique was used to measure the polarization resistance R_p.

After 20 minutes of immersion at free corrosion potential, EIS measurements were conducted by applying an oscillating potential ±5mV around the free corrosion potential to the working electrode using the frequency range 0.001 Hz-5000 Hz. The experimental conditions are listed in Table 2

RESULTS AND DISCUSSION

Before any experiments were conducted by EIS technique in slightly sour environments, a baseline experimental result needed to be established in the absence of H₂S to serve as the reference point in order to better understand the role of H₂S on the corrosion of carbon steel.

For carbon steel X65 in the pH5 H₂S-free saturated CO₂ solution at corrosion potential, the impedance diagram in Figure 2 exhibited a depressed semi-circle at high frequencies indicating a double-layer capacitance, as well as an inductive loop at lowest frequencies. Depressed semi-circle is not uncommon for iron dissolution in acidic media and it was suggested in the literature that the heterogeneous surface roughness and the nonuniform distribution of current density on the surface may be related with it^{1,2}. The Nyquist impedance diagram did not change with respect to immersion time and showed no mass transfer controlled impedance under these conditions; however, it was not a pure charge transfer controlled process either because the inductive loop at low frequencies indicated that the iron dissolution mechanism might occur in two steps involving an adsorbed intermediate. According to Keddam et al.^{3,4}, the inductive loop at the low frequency was related to the relaxation time of the intermediate adsorbed species, (FeHCO₃)⁺_{ad}.

When the mild steel electrode was immersed in the H₂S-free solution, the measured corrosion potential reached stable value around -696 mV within 5-10 minutes. On the other hand, the change of corrosion potential with time in the presence of 100 ppm gaseous H₂S took much longer to stabilize, Figure 3 showed the corrosion rate increasing from original value of -665 mV to -643 mV in 6 hours, but then began to decrease, reaching -649 mV in 22 hours. After that, the corrosion potential started to increase again and stabilized at around -625 mV after 72 hours. This transient phenomenon was also reflected in the change of characteristics of the Nyquist impedance diagram in the presence of 100 ppm gaseous H₂S with respect to immersion time as shown in Figure 4. It was suggested that a metastable sulfide film, mackinawite, might have formed at electrode surface initially via solid-state formation⁵, resulting in a lower corrosion rate of 0.3 mm/year measured by LPR after first 10 hours of immersion (shown in Figure 7). Before mackinawite could transform into the more stable species such as troilite and pyrite^{5,6}, there was a transition period, in which galvanic coupling effect took place and mackinawite could act as a cathode to enhance the corrosion rate, assuming that the mackinawite is a semi-conductive film. This phenomenon could be seen after 22 hours of immersion (shown in Figure 4), where the characteristics of the impedance diagram had changed drastically, charge transfer resistance, R_t decreased to 32 ohm, corresponding to increase of corrosion rate around 0.92 mm/year (shown in Figure 7), which was even greater than the corrosion rate of carbon steel X65 in H₂S-free solution (0.49 mm/year). The semi-circle at high frequencies indicating a double-layer capacity was no longer as depressed, indicating the corrosion process had opened up more active sites on the electrode facilitating uniform distribution of current density on the surface. In addition, two inductive loops observed at low frequency were related to relaxation time of the intermediate adsorbed species such as (FeHCO₃)⁺_{ads}, (FeSH)⁻_{ads} or (FeSH)_{ads}.

Figure 5 showed that as the electrode was further immersed (after 40 hours), the charge transfer resistance, R_t stopped decreasing and stabilized at around 20 ohm, this value was determined by extending the hypothetical semi-circle that was partially overshadowed by the straight line in the lower frequencies to intercept the value at the x-axis. On the other hand, the straight line that was followed by a semi-circle in the lower frequencies extended as the electrode was depressed further. Eventually the impedance diagram stabilized after 48 hours of immersion and no change was observed throughout the rest of

experiment even after 72 hours of immersion time. Figure 6 illustrated that the presence of 100 ppm H₂S had resulted in totally different characteristics of impedance plot at the corrosion potential for steady state conditions.

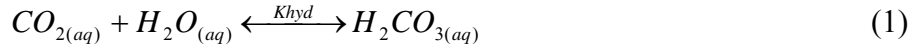
MODELING

In order to interpret the physical meaning of the EIS data, a mechanistic physico-chemical model was built.

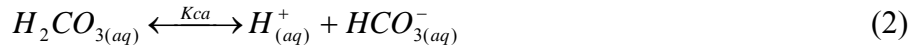
Physical model

The mechanistic model of electrochemical impedance response is based on following fundamental reactions in CO₂ corrosion proposed by previous studies in the field⁷⁻¹⁴:

When CO₂ is dissolved in water, hydration of aqueous carbon dioxide takes place to form carbonic acid:



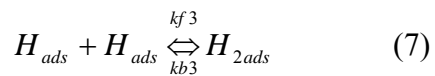
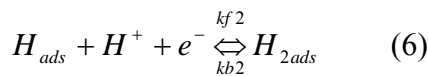
The carbonic acid H₂CO₃ is then dissociated in two steps:



It is proposed that carbonic acid provides a reservoir of H⁺ ions at a given pH. Therefore hydrogen evolution is assumed to be the most dominant cathodic reaction. Whereas the other possibility of direct carbonic acid reduction is not considered in this particular EIS model:⁸



When hydrogen ions H⁺ diffuse through the diffusion boundary layer to the metal surface, hydrogen evolution involving intermediate adsorbed hydrogen atom will take place as shown below:



i.e. as the hydrogen ion is being reduced (5), the resulting adsorbed hydrogen atom H_{ads} can either recombine with another adsorbed hydrogen atom to form H_{2ads} (7), or it has the

possibility to undergo another charge transfer step by reacting with a hydrogen ion and an electron to form H_{2ads} (6). This additional charge transfer reaction (6) is first proposed by Heyrovsky¹⁵ and is also known as Heyrovsky's reaction. On the other hand, the slow recombination reaction (7) assumed by Tafel¹⁶ is the best-known rate determining chemical reaction.

Mathematical model

In order to develop a mechanistic EIS model that gives an electrochemical impedance response, both charge transfer and mass transfer of H^+ need to be taken into consideration. Moreover, hydration of carbon dioxide (1), being the slowest chemical reaction in CO_2 solution, which contributes partly to the current limitation⁹, is also included in the model. The resistance resulting from the current and the overvoltage is impedance and the total impedance response is described as:

$$Z_{total} = \frac{\eta_{total}}{i} = \frac{\eta_{d,B.L.,r} + \eta_t}{i} \quad (8)$$

where

$$i = I \sin(\omega t)$$

I = current amplitude

$$\omega = 2\pi f$$

f = frequency (Hz)

$\eta_{d,B.L.,r}$ = diffusion overvoltage taking account of finite-thickness boundary layer and limiting chemical reaction (1).

η_t = charge transfer overvoltage

Charge-transfer overvoltage

Charge transfer overvoltage arises when charge transfer reaction is rate determining when current flows. Therefore one needs to determine the relationship between current and overvoltage resulting from charge transfer reaction. The two-step charge transfer process with two possible paths of hydrogen evolution as shown above can be modeled by mathematical equations. The reaction for the reduction of hydrogen ions on the bare metal surface (5) can be modeled by the following relationship:

$$i_1 = (1 - \theta)i_{0,1} 10^{(-\eta/b_1)} \quad (9)$$

where

θ = coverage factor, percentage of H_{ad} covered on the metal surface ($0 \leq \theta \leq 1$)

$i_{0,1}$ = exchange current density for hydrogen ion reduction on fully uncovered electrode at equilibrium potential $\approx 1.58 \times 10^{-2} \text{ A/m}^2$ for 20°C and pH5^{7,17}

η = overvoltage = $\varepsilon - \varepsilon_0$

ε_0 = equilibrium potential
 b_1 = Tafel slope = $2.303RT/\alpha_1F$
 α_1 = Symmetry factor, according to Bockris et al. ¹⁷, for hydrogen evolution,
 $\alpha_1=0.5$ giving $b_1=0.108$ at 20°C .

On the other hand, Heyrovsky's reaction (6) requires an adsorbed hydrogen atom to react with a hydrogen ion and an electron. Since this is an electrochemical reaction involving charge transfer, it can be described similarly as above:

$$i_2 = \theta i_{0,2} e^{(-\eta/b_2)} \quad (10)$$

The recombination of H_{ad} is a chemical reaction requiring two adsorbed hydrogen atoms, therefore rate of reaction (7) is modeled as:

$$K_3 = 2Fk_{f3}\theta^2 \quad (11)$$

The rate of change of H_{ad} adsorption coverage θ on the metal surface is described by the fact that reaction of hydrogen ion reduction (5) increases the H_{ad} adsorption coverage, whereas the Heyrovsky's reaction (6) and recombination chemical reaction (7) decrease the adsorption coverage:

$$\frac{d\theta}{dt} = \frac{i_1 - i_2 - K_3}{C_H} \quad (12)$$

where C_H is the constant linking the fraction of the adsorbed surface θ and the surface concentration of adsorbed species expressed in mol/cm^2 . It is also called adsorption capacitance and it is considered to be equal to $10^{-8} \text{ mol}/\text{cm}^2$, which corresponds to about one monolayer for the case of one intermediate bonding to one surface metal atom.³

Combining equation (9), (10), (11) and (12) with the initial condition: $t=0$; $\theta=0$, adsorption coverage can be determined as a function of time $\theta(t)$. Therefore the individual current i_1 , i_2 is a function of overvoltage and adsorption coverage, which is a function of time. The total current resulting from the cathodic charge transfer of hydrogen evolution is the sum of individual current:

$$i_{total} = i_1 + i_2 \quad (13)$$

When small amplitude of sinusoidal alternating current is induced, a relationship between charge transfer overvoltage and current was derived by Gerischer and Mehl:¹⁸

$$\eta_t = \frac{I \sin(\omega t)}{L_D - \frac{ab}{b^2 + C_H^2 \omega^2} + \frac{aC_H \omega}{b^2 + C_H^2 \omega^2} j} \quad (14)$$

Where

$j = \text{imaginary component} = \sqrt{-1}$

$$L_D = \frac{F(\alpha_1 i_1' + \alpha_2 i_2')}{RT}$$

$$a = \frac{F(i_2 - i_1)(\alpha_2 i_2' - \alpha_1 i_1')}{RT}$$

$$b = i_1 + i_2 + 2F\theta' k_{f3}$$

i_1' , i_2' and θ' are values at equilibrium potential.

It is seen in equation (14) that real and imaginary component are both frequency dependent. This frequency dependence was evoked by periodic change of adsorption coverage θ . This charge transfer overvoltage has a phase shift with respect to the alternating current, that's why there is an imaginary component. This imaginary component can be both capacitive ($a > 0$) and inductive ($a < 0$) and it depends on which way the adsorption coverage θ change with the fluctuation of overpotential and whether it increases or decreases the current.

Diffusion overvoltage

Diffusion overvoltage appears when the supply of reactants at the electrode or the removal of the reaction products is rate determining when current flows. When applying a sinusoidal alternating current, a relationship between diffusion overvoltage and sinusoidal alternating current is found by Warburg¹⁹:

$$\eta_w = \frac{RT}{n^2 F^2} \frac{v^2}{\sqrt{\omega} [H^+]_{bulk} \sqrt{D_{H^+}}} I \sin(\omega t - \frac{\pi}{4}) \quad (15)$$

where

$v = \text{stoichiometric constant}$

$[H^+]_{bulk} = \text{concentration of } H^+ \text{ ions in the bulk}$

$D_{H^+} = \text{diffusion coefficient for } H^+ \text{ ions} = 9.312 \times 10^{-5} \text{ cm}^2/\text{sec}$, according to Newman²¹

The diffusion overvoltage lags behind the current by a phase angle of $\pi/4=45^\circ$ and the so-called Warburg Impedance can be determined by:

$$Z_w = \frac{\eta_w}{i} \quad (16)$$

where $i = I \sin(\omega t)$

However, the Warburg impedance is derived assuming an infinite-thickness boundary layer resulting from a stagnant condition, which is rarely encountered in practical applications. Therefore diffusion overvoltage with a finite-thickness boundary layer is more appropriate for the model and it was derived by Sluyters et al²⁰:

$$\eta_{d,bl} = \frac{RT}{n^2 F^2} \frac{1-i}{[H^+]_{bulk} \sqrt{2\omega D_{H^+}}} \tanh \left[\delta \sqrt{\frac{i\omega}{D_{H^+}}} \right] I \sin \omega t \quad (17)$$

where

δ = boundary layer thickness

Equation (17) shows that the phase shift is no longer constant, but is a function of the frequency and the thickness of diffusion boundary layer. Figure 8 demonstrated that the characteristics of the impedance plot for a finite-thickness boundary layer is very different to that of infinite-thickness boundary layer and is strongly dependent on the thickness of boundary layer as shown in Figure 9.

Reaction overvoltage

Reaction overvoltage is a phenomenon resulting from the existence of a slow (rate determining) chemical step in the overall reaction. In the case of CO₂ corrosion, the slow Hydration of CO₂ (1) contributes partly to the limiting current and previous studies^{22,23} suggested that the superposition of diffusion and chemical reaction controlled limiting current is legitimate. Therefore the influence of diffusion and reaction-rate control are treated simultaneously when alternating current is induced and diffusion overvoltage with reaction η_r is obtained by Vetter:²²

$$\eta_r = \frac{RT}{n^2 F^2} \frac{v^2}{\sqrt{\omega} [H^+]_{bulk} \sqrt{2D_{H^+}}} \sqrt{\frac{1 + \left(\frac{k}{\omega}\right)^2 + \frac{k}{\omega}}{1 + \left(\frac{k}{\omega}\right)^2}} I \sin \omega t - \frac{RT}{n^2 F^2} \frac{v^2}{\sqrt{\omega} [H^+]_{bulk} \sqrt{2D_{H^+}}} \sqrt{\frac{1 + \left(\frac{k}{\omega}\right)^2 - \frac{k}{\omega}}{1 + \left(\frac{k}{\omega}\right)^2}} I \cos \omega t \quad (18)$$

This diffusion overvoltage with reaction has a phase shift with respect to alternating current that is not constant, but is a function of the frequency ω and the rate of the

reaction k . Equation (18) without the square root expression would be a diffusion overvoltage (15) that was related to transport of hydrogen ion H^+ . It is this expression that takes into account the formation and depletion of H^+ as a result of the rate-determining step. However, equation (18) was derived for the case of infinite boundary layer condition, because Vetter assumed that the fluid is well mixed and in equilibrium only when $x \rightarrow \infty$, which is a good assumption for laminar flow and truly stagnant solutions. Whereas for a high enough velocity and turbulent flow, one needs to assume that the edge of the mass transfer boundary layer at $x = \delta$ is the point where everything is well mixed and all reactions are in equilibrium. Therefore reaction overvoltage for mass transfer involving rate-determining reaction in turbulent flow conditions is derived by the present authors (see Appendix for full derivation) to be:

$$\eta_{\delta,r} = \frac{RT}{n^2 F^2 [H^+]_{bulk} D_{H^+} \lambda} \tanh(\lambda \delta) I \sin \omega t \quad (19)$$

$$\text{where } \lambda = \sqrt{\frac{i\omega + k}{D_{H^+}}}$$

Combining equation (8), (14) and (19), the total electrochemical impedance Z_{total} for the cathodic reaction in CO_2 corrosion is obtained.

Double layer capacitance

From the impedance spectrum, the semi circle at high frequency that contains information about double layer capacitance, is commonly modeled by a capacitor in a parallel configuration with the total impedance. However, in order to obtain more accurate fit results, the constant phase element (CPE) is substituted for capacitors. The so-called CPE is an element whose impedance value is a function of the frequency and its phase is independent of the frequency. Its impedance is defined as:²⁴

$$Z_{CPE} = \frac{1}{Y_o} (j\omega)^{-n} \quad (20)$$

where Y_o = modulus of CPE,
 ω = angular frequency = $2\pi f$
 n = phase.

The reason that CPE is used instead of capacitors when one analyses the impedance spectra is that most impedance curves measured in experiments are not ideal semi-circles, but are depressed due to heterogeneous surface roughness and the nonuniform distribution of current density on the surface.^{1,2} The depression degree depends on the phase n of the CPE.²⁴

Therefore CPE is the only element in the model that is not mechanistic and it is assumed to be in a parallel configuration with total impedance Z_{total} as shown in Figure 10.

ANALYSIS OF IMPEDANCE DATA BY USING THE MODEL

The transient characteristics in the slightly sour environments of 100 ppm H₂S measured at corrosion potential (Figure 5) can be successfully modeled by initially adjusting the charge transfer properties such as the exchange current density and Tafel slope to match R_t value and then gradually decreasing the diffusion coefficient for H⁺. The good agreement between experimental data and model prediction shown in Figure 11 allowed us to conclude that such phenomenon was related to mass transfer and it implied the formation of the stable sulfide film such as troilite and pyrite. As the stable sulfide film formed, the corrosion process became mass transfer controlled because species such as H⁺ could not diffuse easily to the surface of the electrode to take part in the electrochemical reaction, hence the corrosion rate decreased. Polarization resistance, R_p values that were measured by using LPR technique matched well with the Nyquist plot for the R_p values that intercepted at the real axis, (not the hypothetical R_t), corresponding to the decrease of corrosion rate around 0.55 mm/year. (shown in Figure 7) The tail at the end of the semi-circle at the lowest frequencies was related to limiting chemical reaction rate control such as hydration of carbonic acid or chemisorption of (FeSH⁻)_{ads}.

Hence, the model of electrochemical impedance response developed based on the fundamental equation of electrochemistry was judged as successful as it enabled interpretation the complex physico-chemical phenomena underlying CO₂/H₂S corrosion process.

DISCOVERY OF THE EXPERIMENTAL ERROR

To authors' "surprise", few months following the original series of measurements it was accidentally discovered that a new series of experiments conducted under the same conditions showed very different EIS characteristics. The only difference in the two series of experiments was what was considered a minor modification (improvement) of the experimental set-up. In the original series of experiments, when the mild steel working electrode was mounted on the stainless steel rotating shaft's specimen holder loose electrical contact was obtained. In order to avoid this problem which affected EIS measurements greatly, a thin platinum foil inserted in between to ensure good contact (shown in Figure 12). As this contact area between the specimen and the shaft was meant to be kept "dry" the contact problem appeared to have been successfully solved even if the design was not mechanically robust. Therefore a more robust and precise design was devised by making bottom part of the rotating shaft hollow with an interior conical thread including a thin slit. When a screw was inserted from the bottom end of the rotating shaft, it slightly expanded and made firm contact with the specimen (shown in Figure 13) and eliminated the need to use the thin platinum foil.

Surprisingly, with this setup a completely different EIS plot was obtained (shown in Figure 14). The Nyquist plot no longer demonstrated complex transient characteristics at lower frequencies that were apparently related to mass transfer controlled mechanisms. On the contrary, the new EIS transient characteristics showed only an enlargement of a depressed semi-circle which indicated charge transfer controlled mechanism as the main underlying process. The LPR results were not affected by this change.

With the new modification of experimental set-up, similar phenomenon was also observed at slightly higher concentration of H₂S. One can observe how the depressed semi-circle increases in diameter over time in Figure 15, which demonstrates the transient characteristics of the Nyquist impedance diagram in the presence of 340 ppm gaseous H₂S. The initial EIS measurement (taken after 20 minutes of immersion) suggests that a protective thin sulfide film had formed via solid state formation⁵ at the electrode surface immediately after immersion. The low-frequency data (of the initial EIS measurement) that drifts below the x-axis is not of instrumental error, but indicates the transient increase of polarization resistance (R_p) during the long EIS measurement, hence illustrating the increase of surface coverage over time. By the end of first EIS measurement, the electrode had been immersed in the solution for 4 hours and the lowest frequency ($f=0.001$) data point indicated that R_p was already 394 ohm (denoted by the larger marker), matching a low corrosion rate of 0.08 mm/year (measured by LPR). Comparing to the corrosion rate of H₂S-free solution (0.84 mm/year), this result suggests that mackinawite film had achieved a ten-fold inhibition of corrosion rate within 4 hours of immersion under the experimental condition. The characteristics of the impedance diagram stopped changing after 36 hours of immersion indicating that the sulfide film had reached equilibrium and the corrosion rate remained constant throughout the rest of the experiment.

With the new experimental set-up, more reliable EIS raw data were obtained, which lead to different conclusion about the CO₂/H₂S corrosion process. Instead of a growth of a thick surface film which affects mass transfer, it was concluded that a thin surface film forms that affects charge transfer probably by a surface coverage effect. The latter conclusion was subsequently confirmed by using surface analysis (ESCA).

CONCLUSIONS

- EIS technique presents a large challenge both from a theoretical as well as an experimental point of view.
- Collecting accurate EIS raw data is not easy even if the instruments used nowadays make it appear almost effortless. Obtaining reproducible EIS results does not necessarily guarantee reliable data acquisition. EIS is very sensitive, which is both a blessing and a curse, as it “sees” aspects of the corrosion process that cannot be obtained with DC techniques, but it also picks up problems not seen by other techniques.

- Building mechanistic models to capture the EIS data is a very complex task however, it carries a lot of potential as it enables uncovering of physico-chemical processes underlying corrosion. However, any model is only as good as the empirical data it is using as input.
- A “minor” detail in the experimental set-up described in this study caused erroneous acquisition of EIS raw data. These data were “successfully” modeled by using a complex electrochemical theory, which appeared plausible. When the experimental mistake was discovered the EIS data were retaken, the analysis redone and the conclusions about the corrosion process were completely revised. One year expired in the process.

REFERENCE

1. E. McCafferty, Corros. Sci. 39 (1997) 243.
2. D.D. MacDonald, M.C.H. Mckubre, J.O.M. Bockris, B.E. Conway, R.E. White (Eds.), Modern Aspects of Electrochemistry, vol. 14, Plenum Press, New York, 1982, p.61
3. M. Keddam, O.R. Mattos, H. Takenouti, J. Electrochem. Soc. 128 (1981) p.257.
4. M. Keddam, O.R. Mattos, H. Takenouti, J. Electrochem. Soc. 128 (1981) p.266.
5. D.W. Shoesmith, P. Taylor, M.G. Bailey, D.G. Owen, J. Electrochem. Soc. 127 (1980) p.1007.
6. J.B. Sardisco, W.B. Wright, E.C. Greco, Corrosion 19 (1963) p.354
7. S. Nestic, J. Postlethwaite and S. Olsen, “An Electrochemical Model for Prediction of CO₂ Corrosion”, CORROSION/95, paper no.131
8. C. deWaard and D. E. Milliams, Corrosion, 31 (1975): p.131
9. G. Schmitt and B. Rothman, Werkstoffe und Korrosion, 28 (1977): p.816
10. L.G. S. Gray, B.G. Anderson, M. J. Danysh, P.G. Tremaine, “ Mechanism of Carbon Steel Corrosion in Brines Containing Dissolved Carbon Dioxide at pH 4”, Corrosion/89, paper no. 464, (Houston, TX: NACE International, 1989).
11. L.G. S. Gray, B.G. Anderson, M. J. Danysh, P.G. Tremaine, “ Effect of pH and Temperature on the Mechanism of Carbon Steel Corrosion by Aqueous Carbon Dioxide”, Corrosion /90, paper no.40, (Houston, TX: NACE International, 1990).

12. M. R. Bonis and J.L. Crolet, "Basics of the Prediction of the Risks of CO₂ corrosion in Oil and Gas Wells", Corrosion/89, paper no. 466, (Houston, TX: NACE International, 1989)
13. S. Netic, M. Nordsveen, R. Nyborg and A. Stangeland, "A Mechanistic Model for CO₂ Corrosion with Protective Iron Carbonate Films", CORROSION/2001, paper no. 40, (Houston, TX: NACE International, 2001).
14. S. Netic and K.J. Lee, "The mechanistic model of iron carbonate film growth and the effect on CO₂ corrosion of mild steel", Paper No.237, CORROSION/02
15. J. Heyrosky, Rec. Trav. Chim. Pays-Bas 44, 499 (1925)
16. J. Tafel, Z. Physik, Chem. 50, (1905): p641
17. J.O.M. Bockris, D. Drazic and A.R. Despic, Electrochimica Acta, 4 (1961): p.325
18. H. Gerischer and W. Mehl, Z. physik. Chem (1955): p.1049
19. E. Warburg, Wied. Ann. 67, (1899): p.493
20. M. Sluyters-Rembach and J.H. Sluyters, in Electroanalytical Chemistry, Vol. 4 (A. J. Bard, ed.), Marcel Dekker, New York, 1970
21. J.S. Newman, Electrochemical Systems, 2nd Edition, (Prentice Hall, Englewood Cliffs, New Jersey, 1991)
22. K.J. Vetter, Electrochemische Kinetik, p 256 (Springer-Verlag, Berlin, 1961)
23. S. Netic, B.F.M. Pots, J. Postlethwaite and N. Thevenot, "Superposition of diffusion and chemical reaction controlled limiting currents – application to CO₂ corrosion", J. Corrosion science and engineering, ISSN 1466-8858, (1995)
24. J.E. Ferrer, L. Victori, Electrochim. Acta 39 (1994) p 581
25. K.J. Vetter, Electrochemische Kinetik, p 237 (Springer-Verlag, Berlin, 1961)

APPENDIX

In order to derive reaction impedance with a finite boundary layer, one needs to consider the following sequence of reactions:

When CO₂ is dissolved in water, hydration of aqueous carbon dioxide takes place to form carbonic acid:



The carbonic acid H₂CO₃ is then dissociated in two steps:



It is proposed that carbonic acid provides a reservoir of H⁺ ions at a given pH. Therefore hydrogen evolution is assumed to be the most dominant cathodic reaction.



The hydrogen ions H⁺ discharged in the cathodic evolution of hydrogen gas (24) are replaced by dissociation of the carbonic acid. Although the dissociation reactions (22) (23) are inherently fast, the formation of carbonic acid via the hydration step of aqueous carbon dioxide (21) is rate determining and causes the overvoltage of homogeneous reaction.

Hence Fick's second law in the form

$$\frac{\partial c}{\partial t} = D \frac{\partial^2 c}{\partial x^2} + \nu \quad (25)$$

is applied for the change with time (t) and distance (x) of H⁺ concentration as a result of the diffusion and reaction processes.

Vetter²⁵ proposed the relation for formulation of the homogeneous reaction rate ν ,

$$\nu = \nu_0 \left[1 - \left(\frac{c}{\bar{c}} \right)^p \right] \quad (26)$$

with reaction order p, concentration c and bulk concentration \bar{c} . For the evaluation of the reaction impedance only the current and overvoltage range in which a linear relationship

exists between current i and overvoltage η is of interest. This is true only for relatively small concentration changes²⁵.

Since

$$\left(\frac{c}{\bar{c}}\right)^p = \left(1 + \frac{c - \bar{c}}{\bar{c}}\right)^p \approx 1 + p \frac{c - \bar{c}}{\bar{c}} \quad (27)$$

the following is approximately valid:

$$v = -\frac{v_0 p}{\bar{c}} \Delta c = -k \Delta c \quad (28)$$

where $\Delta c = c - \bar{c}$ and $k = \frac{v_0 p}{\bar{c}}$

The reaction order in this case is $p=1$. v_0 is the rate at which the two opposing reactions meet to establish equilibrium and may therefore be designated as the reaction exchange rate.

Substituting equation (28) for the reaction rate into equation (25) gives the partial differential equation

$$\frac{\partial \Delta c}{\partial t} = D \frac{\partial^2 \Delta c}{\partial x^2} - k \Delta c \quad (29)$$

for the concentration difference $\Delta c(x,t) = c(x,t) - \bar{c}$ where \bar{c} = bulk concentration (=H⁺ in this case)

An alternating current density of frequency $\omega/2\pi$, i.e.

$$i = I \sin \omega t \quad (30)$$

which satisfies the boundary condition at the surface

$$\left(\frac{\partial \Delta c}{\partial x}\right)_{x=0} = -\frac{1}{nFD} I \sin \omega t \quad (31)$$

In addition, a boundary condition for a finite diffusion boundary layer is also satisfied

$$\Delta c_{x=\delta} = 0 \quad \text{where } \delta = \text{diffusion boundary layer} \quad (32)$$

As well as the initial condition

$$\Delta c(x,0) = 0 \quad \text{for all } x \quad (33)$$

Using separation of variable method, one starts by looking for product solutions of the form

$$\Delta c(x,t) = X(x)T(t) \quad (34)$$

where $X(x)$ is a function of x alone and $T(t)$ is a function of t alone. Plugging into the modified partial differential equation of Fick's second law (29), one obtains

$$XT' = DX''T - kXT \quad (35)$$

After separating the variables, the equation is now in the form of

$$\frac{T'}{T} = \frac{DX''}{X} - k \quad (36)$$

For the equality to hold, one must have

$$\frac{T'}{T} = \alpha \quad \text{and} \quad \frac{DX''}{X} - k = \alpha$$

where α is the separation constant. From these equations, one obtains two ordinary differential equations

$$T' - \alpha T = 0 \quad (37)$$

and

$$DX'' - (k + \alpha)X = 0 \quad (38)$$

Separating variables in the boundary condition(32), one get

$$X(\delta)T(t) = 0 \quad (39)$$

If $X(\delta) \neq 0$, then $T(t)$ must be 0 for all t , if so, $\Delta c(x,t) = X(x)T(t) = 0$. To avoid trivial solutions we set

$$X(\delta) = 0 \quad (40)$$

Hence one obtains the boundary value problem in X :

$$DX'' - (k + \alpha)X = 0, \quad X(\delta) = 0$$

with characteristic equation

$$D\lambda^2 - (k + \alpha) = 0 \quad (41)$$

one obtains the distinct real characteristic roots of $\lambda_1 = \sqrt{\frac{(k + \alpha)}{D}}$ and $\lambda_2 = -\sqrt{\frac{(k + \alpha)}{D}}$

Therefore the general solution of X of this differential equation is given as

$$X = C_1 e^{\lambda x} + C_2 e^{-\lambda x} \quad (42)$$

By applying the boundary condition (32),

$$0 = C_1 e^{\lambda \delta} + C_2 e^{-\lambda \delta} \quad (43)$$

$$C_1 e^{\lambda \delta} = -C_2 e^{-\lambda \delta} \quad (44)$$

$$C_1 = -C_2 \frac{e^{-\lambda \delta}}{e^{\lambda \delta}} \quad (45)$$

substitute C_1 into the general solution(42) for space domain, one obtains

$$X(x) = -C_2 \frac{e^{-\lambda \delta}}{e^{\lambda \delta}} e^{\lambda x} + C_2 e^{-\lambda x} \quad (46)$$

$$X(x) = -C_2 \frac{e^{-\lambda \delta}}{e^{\lambda \delta}} e^{\lambda x} + C_2 e^{-\lambda x} \frac{e^{\lambda \delta}}{e^{\lambda \delta}} \quad (47)$$

$$X(x) = \frac{C_2}{e^{\lambda \delta}} \left(e^{\lambda(\delta-x)} - e^{-\lambda(\delta-x)} \right) \quad (48)$$

On the other hand, for the time domain,

$$T' - \alpha T = 0 \quad (49)$$

Let's set $\alpha = i\omega$, one obtains

$$T' - i\omega T = 0 \quad (50)$$

The general solution for the above differential equation for time domain is then given as

$$T(t) = Ae^{i\omega t} \quad (51)$$

Combining the two general solutions together, one obtains the general solution of equation (29)

$$\Delta c = X(x)T(t) = \frac{C_2}{e^{\lambda\delta}} \left(e^{\lambda(\delta-x)} - e^{-\lambda(\delta-x)} \right) Ae^{i\omega t} \quad (52)$$

By partial differentiation of the above equation with respect to x and t , and by substituting into partial differential equation (29) of the modified Fick's second law, the coefficient λ can be obtained

$$\begin{aligned} i\omega \frac{C_2}{e^{\lambda\delta}} \left(e^{\lambda(\delta-x)} - e^{-\lambda(\delta-x)} \right) Ae^{i\omega t} &= D\lambda^2 \frac{C_2}{e^{\lambda\delta}} \left(e^{\lambda(\delta-x)} - e^{-\lambda(\delta-x)} \right) Ae^{i\omega t} \\ &\quad - k \frac{C_2}{e^{\lambda\delta}} \left(e^{\lambda(\delta-x)} - e^{-\lambda(\delta-x)} \right) Ae^{i\omega t} \end{aligned} \quad (53)$$

After canceling out the Δc term from the above equation, one obtains

$$i\omega = D\lambda^2 - k \quad (54)$$

Thus

$$\lambda = \sqrt{\frac{i\omega + k}{D}} \quad (55)$$

On the other hand, separating variables in the initial condition, one gets

$$X(x)T(0) = 0 \quad (56)$$

Since $X(x) \neq 0$, $T(0) = 0$

$$0 = Ae^0 \quad (57)$$

If $A=0$, $T(t)=0$ and $\Delta c=0$. To avoid trivial solution, one need to make use of Euler's identity

$$Ae^{i\omega t} = A(\cos \omega t + i \sin \omega t) \quad (58)$$

Now applying the initial condition, one obtains

$$0 = A(\cos 0 + i \sin 0) \quad (59)$$

In order for the above equation to hold true, the $\cos\omega t$ term must be omitted.

$$T(t) = i A \sin\omega t \quad (60)$$

However, for the purpose of mathematical simplicity, the general solution of $T = Ae^{i\omega t}$ is used for the determination of the coefficient C_2 , which can be obtained by applying the boundary condition at the surface(31)

$$\frac{C_2}{e^{\lambda\delta}} \left(-\lambda e^{\lambda(\delta-x)} - \lambda e^{-\lambda(\delta-x)} \right)_{x=0} A e^{i\omega t} = -\frac{1}{nFD} I \sin\omega t \quad (61)$$

$$-\lambda \frac{C_2}{e^{\lambda\delta}} \left(e^{(\lambda\delta)} + e^{-(\lambda\delta)} \right) A e^{i\omega t} = -\frac{1}{nFD} I \sin\omega t \quad (62)$$

After applying the hyperbolic identity $\cosh(x) = \frac{e^x + e^{-x}}{2}$ and canceling $I \sin\omega t$ term on both sides(since $Ae^{i\omega t} = I \sin\omega t$), C_2 is then obtained

$$C_2 = \frac{e^{\lambda\delta}}{\lambda nFD 2 \cosh(\lambda\delta)} \quad (63)$$

Finally, substituting the coefficients C_2 and applying the hyperbolic identity $\sinh(x) = \frac{e^x - e^{-x}}{2}$ into the general solution in equation (52)

$$\Delta c = \frac{\sinh[(\delta - x)\lambda]}{\lambda nFD \cosh(\delta\lambda)} I e^{i\omega t} \quad (64)$$

where $\lambda = \sqrt{\frac{i\omega + k}{D}}$

The objective of the above concentration derivation is to calculate $c(0,t)/\bar{c}$ at the surface. It was assumed that $|\Delta c|/\bar{c} \ll 1$ and thus $c/\bar{c} \approx 1$. Therefore the following relation for the reaction overvoltage is approximately valid²²

$$\eta_r = \varepsilon - \varepsilon_0 = \frac{RT}{nF} \ln \frac{c(0,t)}{\bar{c}} \approx \frac{RT}{nF} \frac{\Delta c(0,t)}{\bar{c}} \quad (65)$$

After Substituting equation (64) for Δc with $x=0$ into the above equation (65) and applying the trigonometric identity $\tanh(x)=\sinh(x)/\cosh(x)$, the reaction overvoltage is obtained:

$$\eta_r = \frac{RT}{n^2 F^2 \bar{c} D \lambda} \tanh(\lambda \delta) I \sin \omega t \quad (66)$$

$$\text{where } \lambda = \sqrt{\frac{i\omega + k}{D}}$$

Table 1. Chemical composition of the X65 carbon steel used for the working electrode (mass%)

C	Mn	Si	Nb	V	Fe	P	S	Cr	Cu	Ni	Mo	Al
0.150	1.34	0.24	0.03	0.055	Balanced	0.011	0.004	0.011	0.01	0.02	0.103	0.032

Table 2. Experimental conditions

Test solution	Water + 3 mass% NaCl
Test material	Carbon steel: X65
Temperature	20°C
Pressure	1 bar
pH	5
Fe ⁺⁺	<1 ppm
Velocity	1000 rpm
Gaseous H ₂ S concentration in CO ₂	0, 3, 100 ppm
Sweep rate	0.125 mV/s
Polarization resistance	From -5 to +5 mV vs. E _{oc}
Potentiostatic EIS	
DC current	0, +100 mV and -100 mV vs. E _{corr}
AC potential	±5 mV
Frequency range	0.001 – 5000 Hz
Test duration	4 – 72 hours

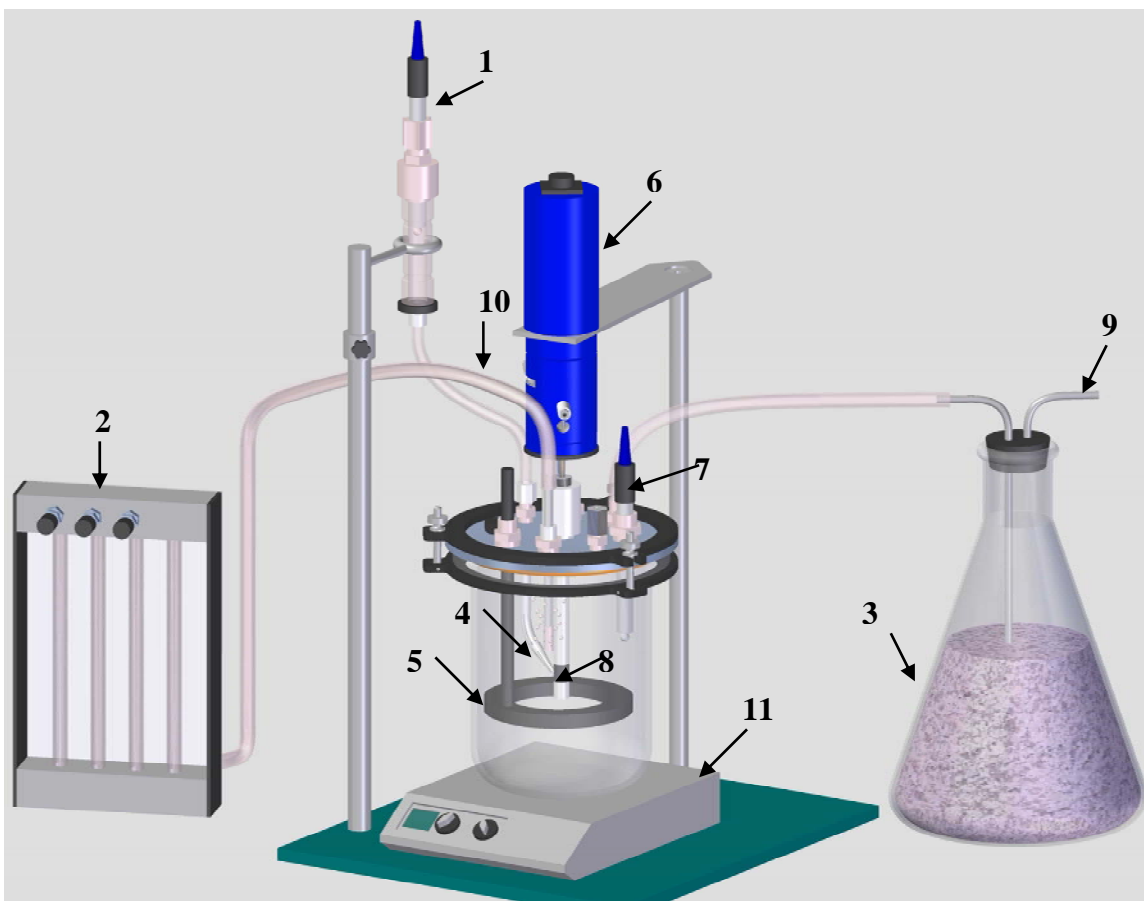


Figure 1. Schematic of the experimental test cell: 1-Ag/AgCl reference electrode, 2-gas rotameter, 3-H₂S scrubber (gas absorbent) , 4-Luggin capillary, 5-graphite counter electrode, 6-rotator, 7-pH electrode, 8-working electrode, 9-gas out, 10-gas in, 11-temperature control unit/stirrer.

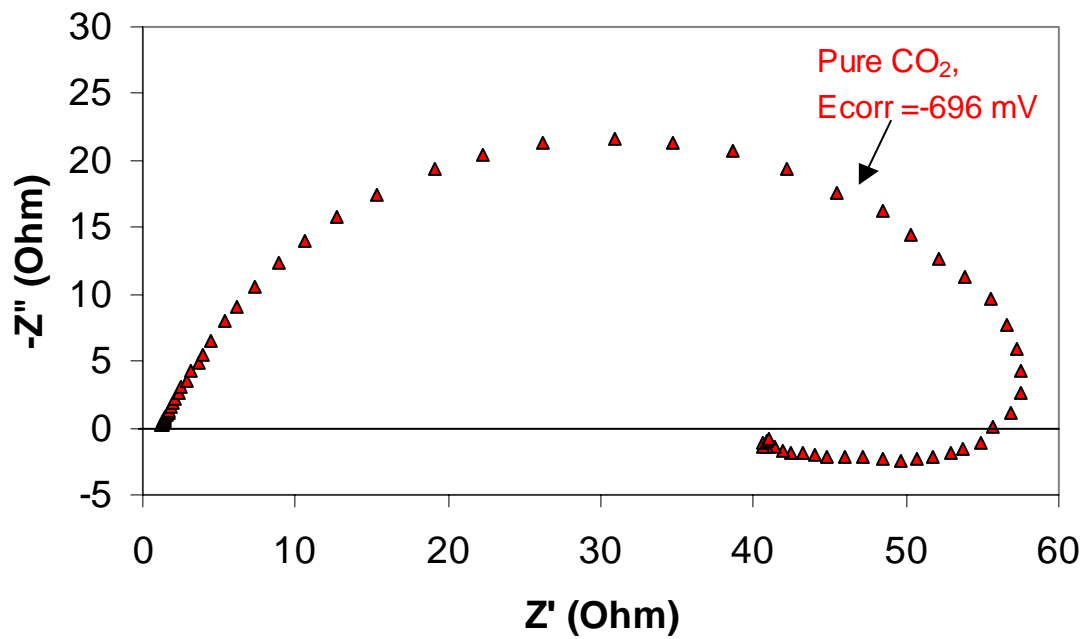


Figure 2. Nyquist impedance diagram for carbon steel X65 in pH5 saturated CO₂ solution of water + 3%NaCl, p=1 bar, t=20⁰C, ω=1000rpm at corrosion potential (vs.Ag/AgCl).

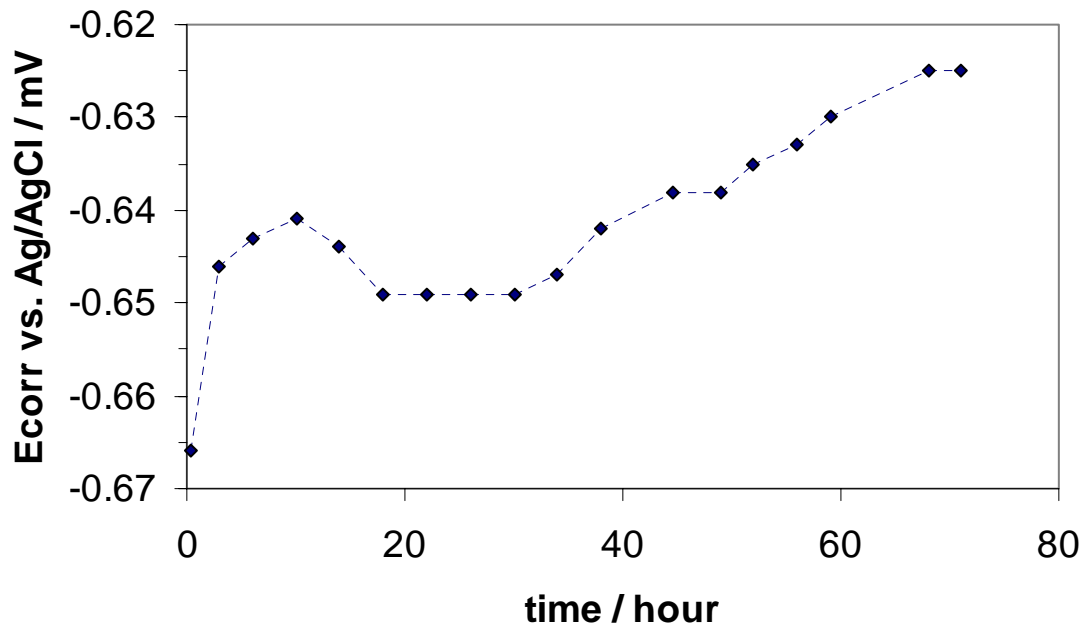


Figure 3. Corrosion potential with respect to immersion time for carbon steel X65 in pH5 saturated CO₂ solution with 100 ppm gaseous H₂S in water + 3%NaCl, p=1 bar, t=20⁰C, ω=1000rpm.

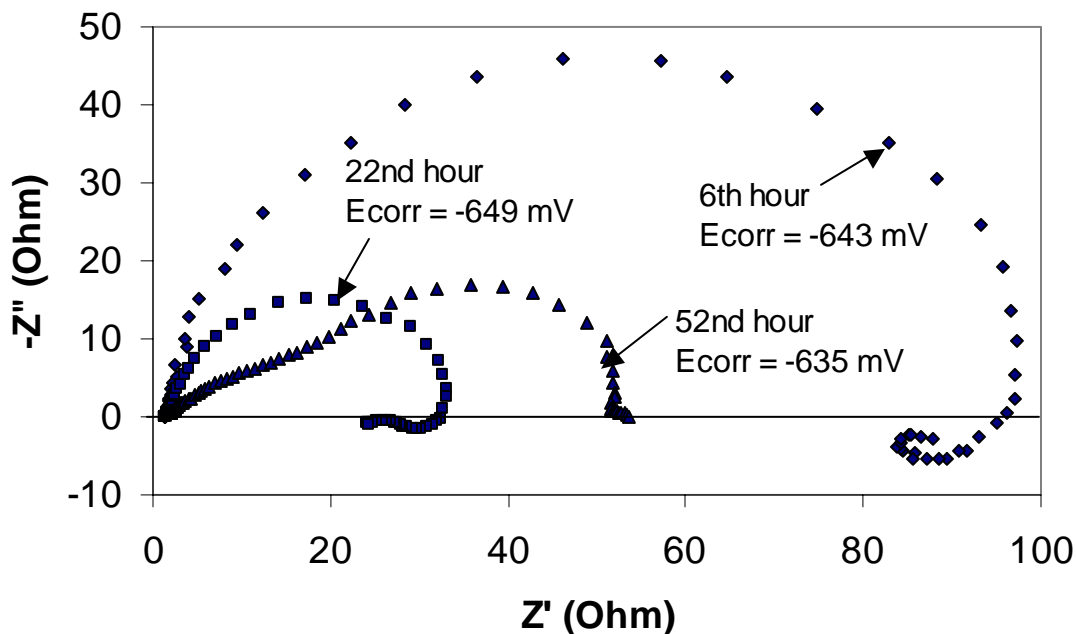


Figure 4. Effect of immersion time on the Nyquist impedance diagram of carbon steel X65 in pH5 saturated CO₂ solution with 100 ppm gaseous H₂S, water + 3%NaCl, p=1 bar, t=20⁰C, ω= 1000rpm at corrosion potential (vs. Ag/AgCl) during the same experiment.

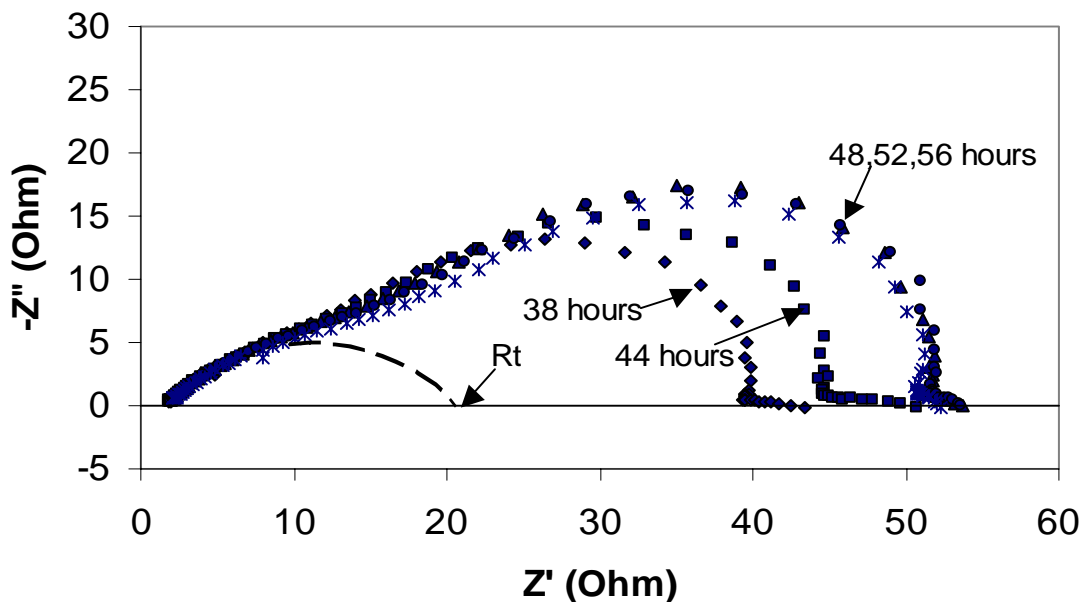


Figure 5. Magnification of the above Figure 4; effect of immersion time (after 40 hours) on the Nyquist impedance diagram of carbon steel X65 in pH5 saturated CO₂ solution with 100 ppm gaseous H₂S, water + 3%NaCl, p=1 bar, t=20⁰C, ω= 1000rpm at corrosion potential (vs. Ag/AgCl)

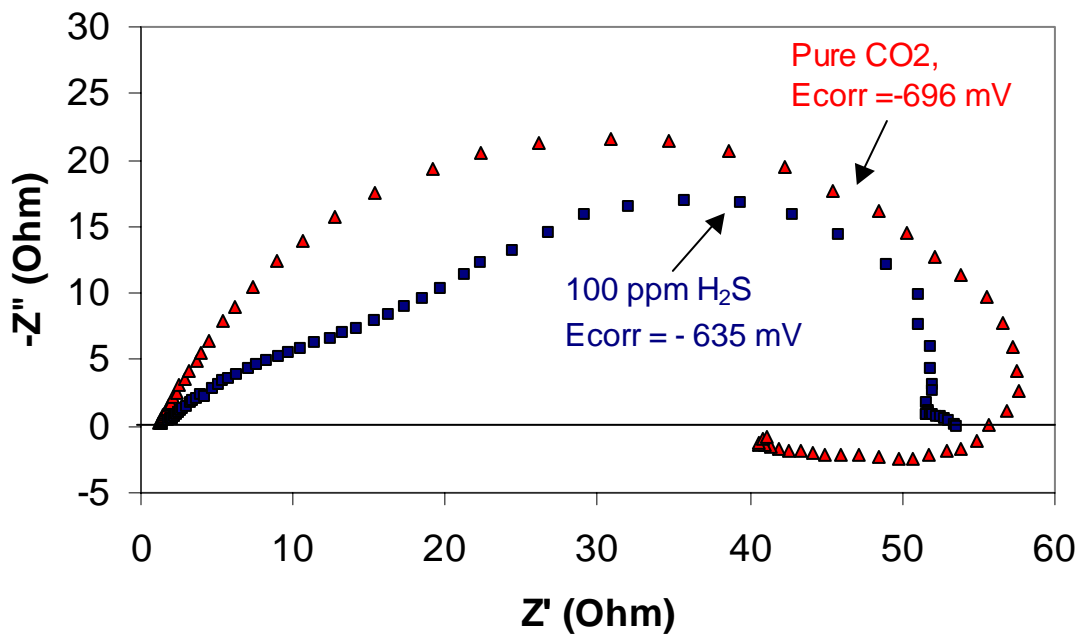


Figure 6. Effect of 100 ppm gaseous H_2S on the Nyquist impedance diagram at steady state condition for carbon steel X65 in pH5 saturated CO_2 solution of water + 3%NaCl, $p=1$ bar, $t=20^{\circ}C$, $\omega=1000rpm$ at corrosion potential (vs. Ag/AgCl).

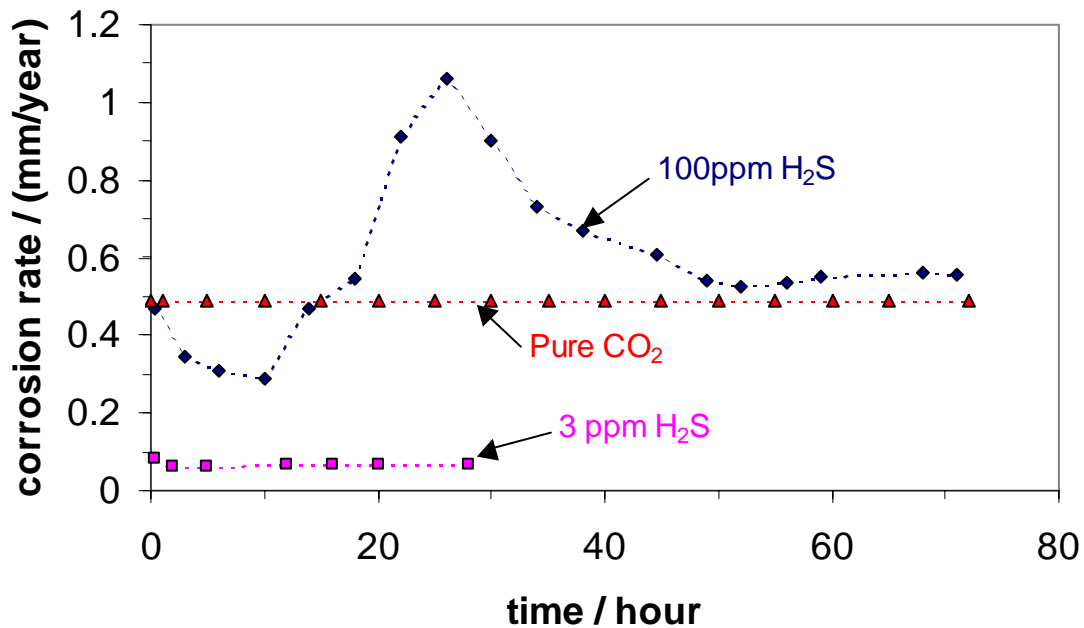


Figure 7. Effect of H_2S gaseous concentration on the corrosion rate (measured by LPR) of carbon steel X65 in pH5 saturated CO_2 solution, water + 3%NaCl, $p=1$ bar, $t=20^{\circ}C$, $\omega=1000rpm$ with respect to immersion time.

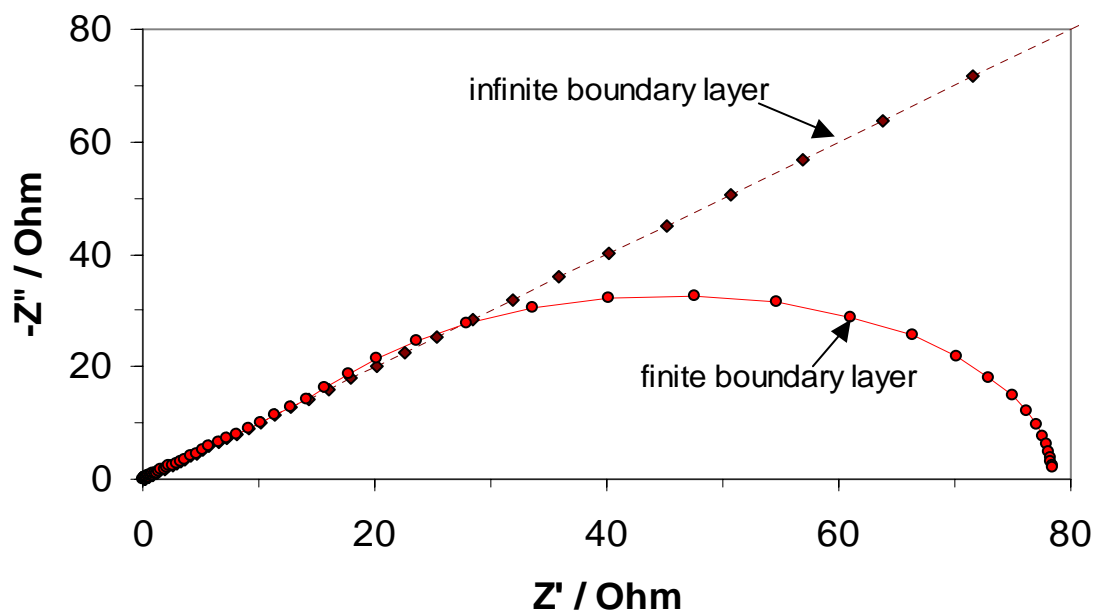


Figure 8. Comparison between calculated electrochemical impedance of H⁺ ions for a finite-thickness diffusion boundary layer, $\delta_{B.L.}=0.003\text{m}$ and infinite-thickness diffusion boundary layer, also known as Warburg impedance, for T=20°C, $[H^+]_{bulk}=1\times 10^{-5}$ mol/liter

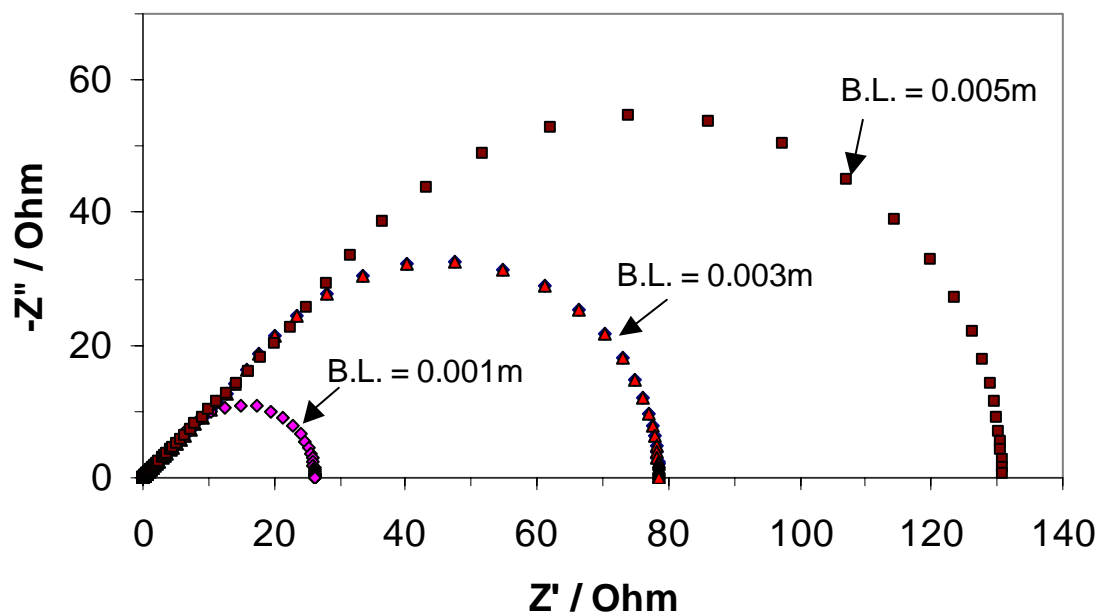


Figure 9. Effect of the thickness of diffusion boundary layer on the characteristics of electrochemical impedance of H⁺ ions for T=20°C, $[H^+]_{bulk}=1\times 10^{-5}$ mol/liter

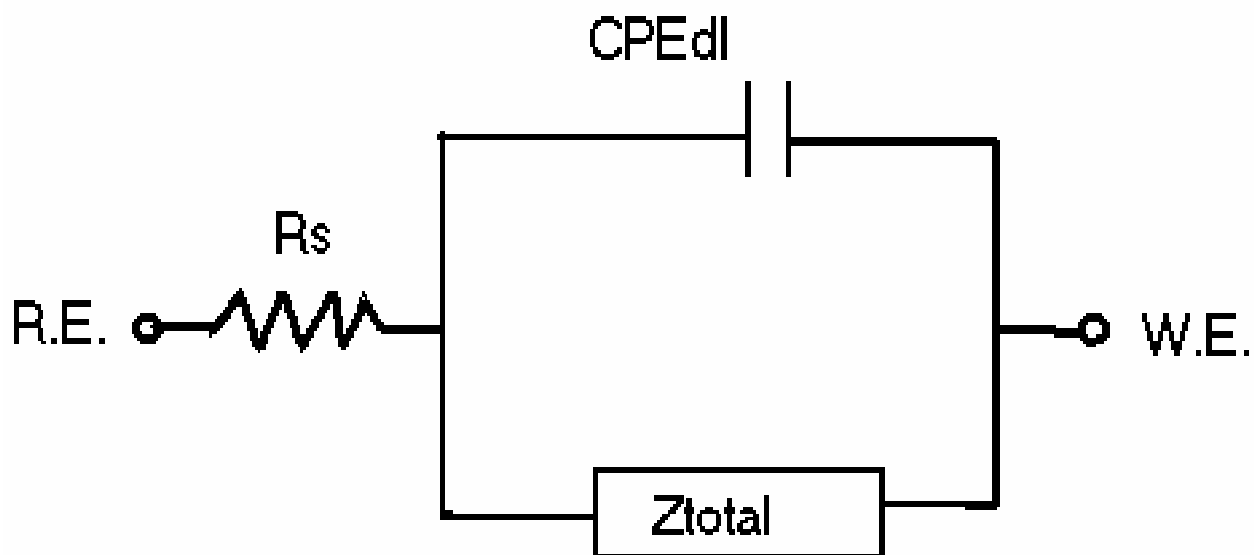


Figure 10. The equivalent circuit of the EIS model. R_s = solution resistance, CPE_{dl} = constant phase elements describing double layer capacitance, Z_{total} = total impedance, R.E. = reference electrode, W.E. = working electrode.

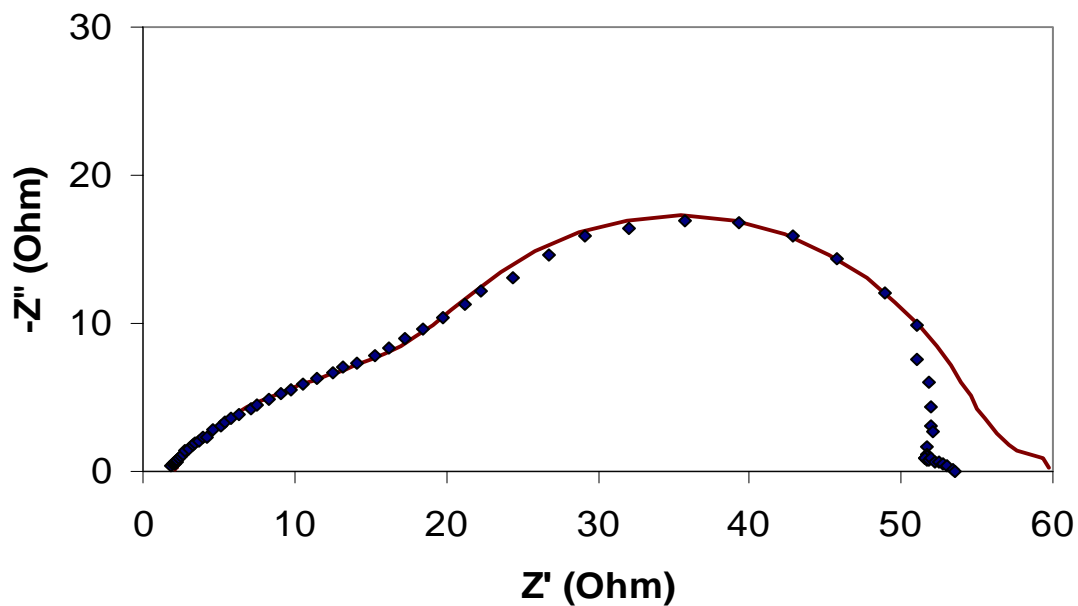


Figure 11. Comparison between experimental data (points) and model prediction (line) for 100 ppm gaseous H_2S in CO_2 , water + 3%NaCl, $p=1$ bar, $t=20^{\circ}C$, $\omega=1000$ rpm at corrosion potential (vs. Ag/AgCl).

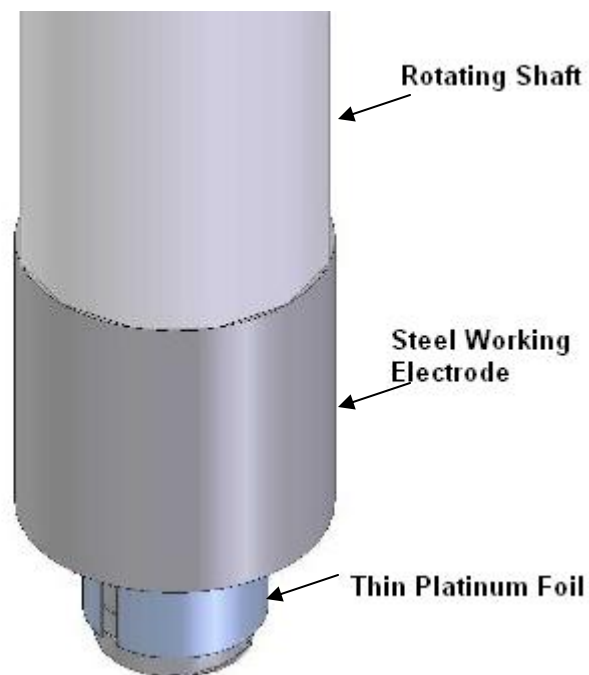


Figure 12. Schematics of old design specimen holder section of rotating shaft

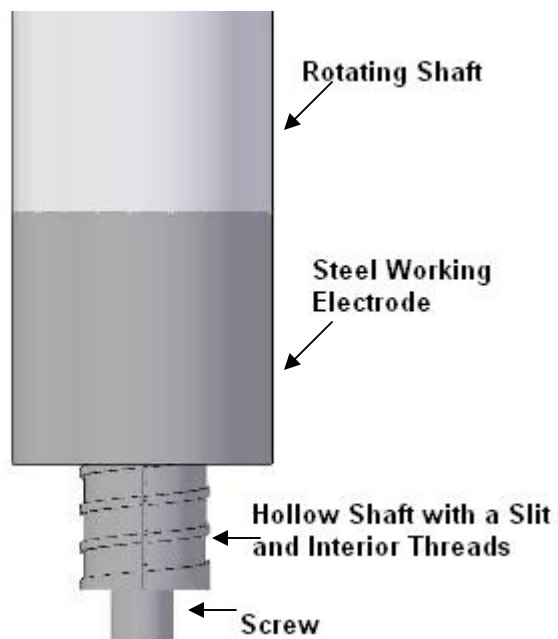


Figure 13. New modification of specimen holder section of rotating shaft

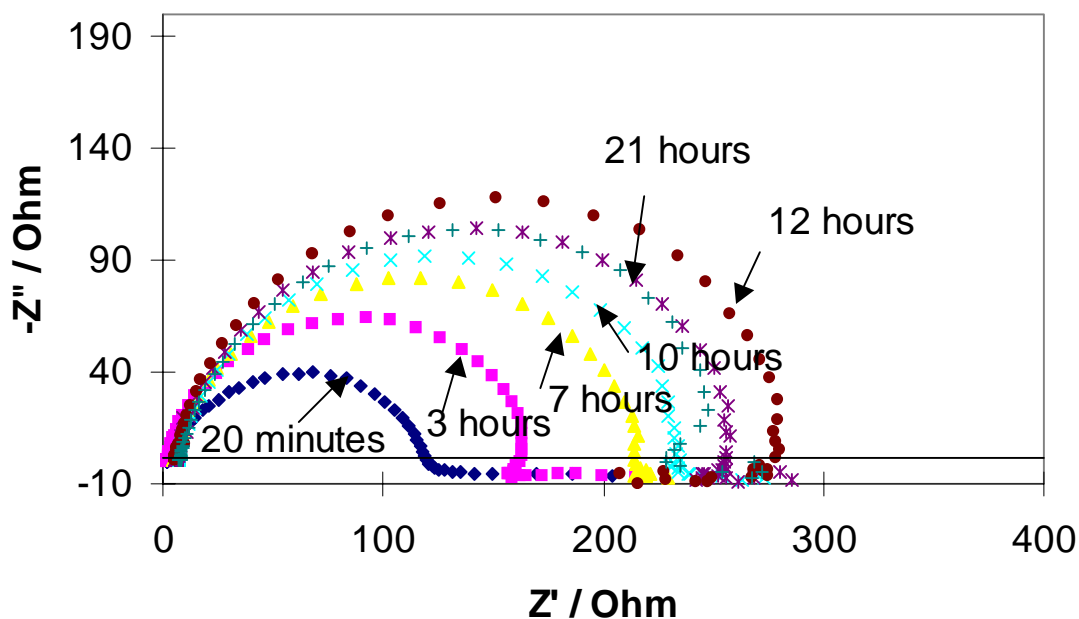


Figure 14. Effect of immersion time on Nyquist impedance diagram of carbon steel X65 in pH 5 saturated CO_2 solution with 100 ppm gaseous H_2S , water + 3% NaCl, $p = 1$ bar, $t = 20^\circ\text{C}$, $\omega = 1000$ rpm at corrosion potential.

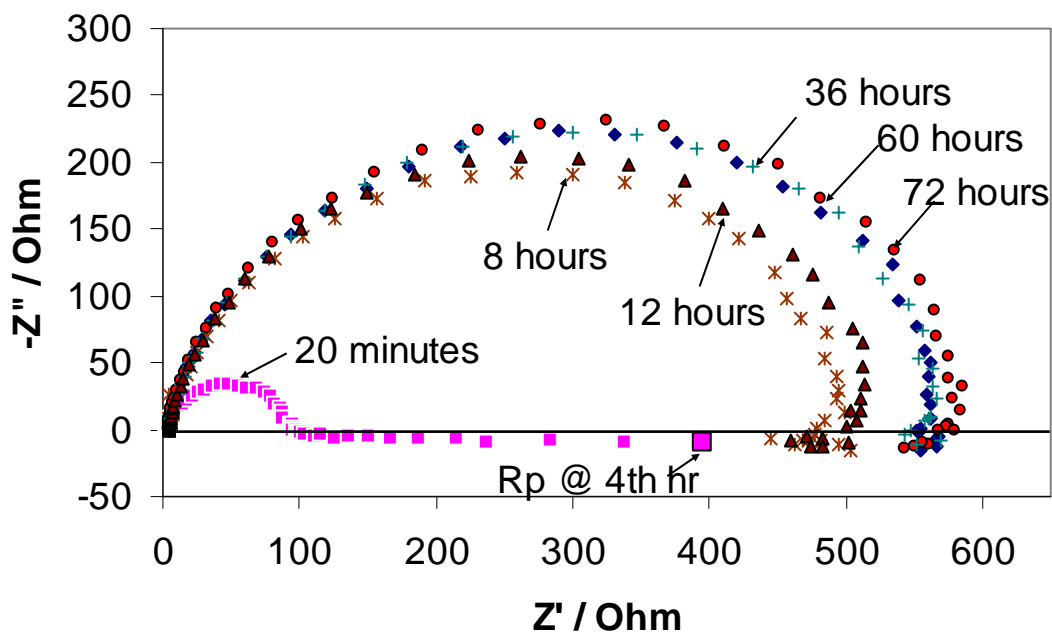


Figure 15. Effect of immersion time on Nyquist impedance diagram of carbon steel X65 in pH 5 saturated CO_2 solution with 340 ppm gaseous H_2S , water + 3% NaCl, $p = 1$ bar, $t = 20^\circ\text{C}$, $\omega = 1000$ rpm at corrosion potential.